Solvent Effects on Conformational Dynamics of Zn-Substituted Myoglobin Observed by Time-Resolved Hole-Burning Spectroscopy†

Yutaka Shibata,*,‡ Atusi Kurita, and Takashi Kushida§

Department of Physics, Faculty of Science, Osaka University, Toyonaka, Osaka 560-0043, Japan

Received July 1, 1998; Revised Manuscript Received October 20, 1998

ABSTRACT: Equilibrium conformational fluctuation of Zn-substituted myoglobin (ZnMb) has been studied in the nanosecond to millisecond time region and 180−300 K temperature region by the time-resolved transient hole-burning spectroscopy. In this technique, the conformational fluctuation of the protein is observed as the temporal variation of the hole spectrum burned by irradiation of the laser pulse. ZnMb solution samples in various solvent conditions were prepared and investigated to elucidate the solvent effect on the conformational dynamics of Mb. The configuration coordinate model assuming the harmonic energy landscape has given a fairly good description of the time dependence of the hole spectra. The observed temporal behavior of both the hole shift and the hole broadening was well expressed by the same stretched exponential correlation function with a rather small and almost temperature-independent β of 0.26. It was found that the correlation time τ_c of the conformational fluctuation of ZnMb determined by this analysis depends linearly on the solvent viscosity regardless of the solvent composition and temperature. This means the almost 0 activation energy for the fluctuation process and can not be understood by simply assuming the Arrhenius-type crossing of the barriers separating the conformational substates. It is shown that this linear viscosity dependence of τ_c, as well as the temperature-independent β, is qualitatively explained in the framework of the hierarchically constrained dynamics (HCD) model [Palmer, R. G. et al. (1984) *Phys. Rev. Lett. 53*, 958−961] with the postulate that the dynamics in the lowest level in the HCD model corresponds in the actual system to the configuration fluctuations of the solvent molecules surrounding the protein.

It is widely accepted that a protein molecule has a flexible conformation and there exist many local minimums, that is, the so-called conformational substates (CS's),[1] on its potential surface (*1*). Conformational motions that correspond to the transitions among CS's may cause relatively large displacements of atoms, and thus have particular importance in biological functioning. Here, we call these transitions among the CS's "diffusive conformational motions". In the case of myoglobin (Mb), which is one of the most intensively studied proteins, hierarchical arrangements of CS's have been confirmed by many cryogenic studies (*2*−*6*). However, in spite of intensive and continuous investigations following the pioneering work by Austin et al. (*7*), it has not yet been clarified how this hierarchy of the potential surface affects the conformational dynamics of proteins at physiological temperatures. In addition, the solvent effect on the diffusive conformational motion of a protein should also be investigated more intensively, since it is considered to have a critical influence on the protein dynamics at physiological temperatures. To shed light on these problems, it is quite important to make direct time-domain observations of the diffusive conformational motions of proteins in a relatively high temperature region. In spite of its great importance, there have been only a few reports on such observations contrary to the intensive cryogenic studies and reaction kinetics studies in which the dynamical effect is reflected only indirectly on the experimental results.

So far, a few time-domain observations of the conformational dynamics of proteins mentioned above have been carried out mainly on carbonmonoxide myoglobin (MbCO) by means of modified flashphotolysis techniques, such as wavelength-resolved flashphotolysis in visible region (*8*, *9*) and in near-infrared region (*10*, *11*), double-pulse flashphotolysis (*12*), time-resolved Raman spectroscopy (*13*), and so on. In the wavelength-resolved flashphotolysis, information about the conformational relaxation after the cutting of the ligand−heme bond is obtained from the temporal variation of the optical absorption spectrum after the photolysis. Ansari et al. derived a stretched-exponential-type ($\exp[-(kt)^{\beta}]$) conformational relaxation of MbCO in the course of the CO-rebinding process by analyzing the observed time-dependent absorption difference spectra through a singular-value decomposition procedure. They clarified that the solvent−viscosity dependence of the determined relaxation rate can be adequately expressed by a modified Kramers equation

† This work was supported by the Research Fellowships of the Japan Society for the Promotion of Science for Young Scientists.

* To whom correspondence should be addressed.

‡ Present Address: Institute for Laser Technology, c/o Kansai Electric Power Company, 3-11-20, Nakoji, Amagasaki, Hyogo 661-0974, Japan.

§ Present Address: Graduate School of Materials Science, Nara Institute of Science and Technology, Ikoma, Nara 630-0101, Japan.

[1] Abbreviations: ZnMb, Zn-substituted myoglobin; CS, conformational substate; TRTHB, time-resolved transient hole burning; TRF, time-resolved fluorescence; PVA, poly-vinyl-alcohol; YAG, yttrium-aluminum-garnet; CW, continuous wave; CCD, charge coupled device; CC, configuration coordinate; UV, ultraviolet; CD, circular dichroism; HCD, hierarchically constrained dynamics.

10.1021/bi9815694 CCC: $18.00
Published on Web 01/22/1999

$$k = \frac{A}{\eta + \sigma} \exp(-H/k_B T) \quad (1)$$

where k_B, T, η, and H are the Boltzmann's constant, the absolute temperature, the solvent viscosity, and the average barrier height separating CS's, respectively. An additional term σ represents the contribution of the protein to the total friction. In a double-pulse flashphotolysis experiment on MbCO, the interconversion rate among the conformers with different geminate CO-rebinding rates is obtained. By using this technique, Tian et al. determined the interconversion rate between the so-called open conformer with a faster rebinding rate and the closed conformer with a slower one in MbCO. They found that the viscosity dependence of this rate can also be expressed by an expression analogous to eq 1, although the obtained interconversion rate was about 2 orders of magnitude slower than the relaxation rate reported by Ansari et al.

In these studies H in eq 1 has not been discussed deeply in spite of its importance for the elucidation of the energy landscape of the protein. It has been established that Mb shows quenching of the conformational fluctuation below ~200 K (*3*, *14*, *15*). This glass-like transition of Mb is considered to be closely connected with the value of H. If this value is sufficiently large, temperature rather than the solvent viscosity chiefly affects the conformational dynamics. On the other hand, in the case of small H, temperature has only a secondary effect on the conformational dynamics of the protein, and the glass-like transition is mainly induced by the vitrification of the surrounding solvent. Thus, H has a close relation to the problem whether the quenching of the conformational dynamics of the protein by lowering temperature is an intrinsic phenomenon of proteins or a solvent-induced phenomenon, which still remains a controversial problem (*3*, *16*, *17*).

Recently, we have made the first time-domain observation of the equilibrium conformational fluctuation of Zn-substituted myoglobin (ZnMb), in which Fe-protoporphyrin IX is replaced with Zn-protoporphyrin IX, by using a novel technique of time-resolved transient hole-burning (TRTHB) spectroscopy (*18*, *19*). This method is one of the most powerful tools for the time-domain observation of protein dynamics. The principle of the measurement is shown in Figure 1, where the absorption spectrum is expressed by the sum of the spectra of many chromophores. Each single chromophore has a different resonance energy depending on the conformation of the apoprotein surrounding the chromophore on account of the chromophore−apoprotein interaction. The conformational fluctuation induces the time-dependent fluctuation of the resonance energy of the chromophore. By detecting this "spectral diffusion", one can make a time-domain observation of the conformational fluctuation in the apoprotein. In the TRTHB method, this is done by detecting the temporal change in the transient hole-burning (THB) spectrum burned by the irradiation of a laser pulse (*20*). The chromophores selectively excited by the laser irradiation are accumulated in a long-living triplet state through the internal conversion, and then a hole is formed around the laser frequency in the absorption spectrum. The hole spectrum varies with time because of the spectral diffusion which reflects the conformational fluctuation of the protein. Since the lifetime of the hole corresponds to that of the triplet state which usually lies in a millisecond region, the conformational fluctuation over a very wide time range of nanosecond to millisecond can be observed by the TRTHB method using a nanosecond-pulse laser for the hole burning.

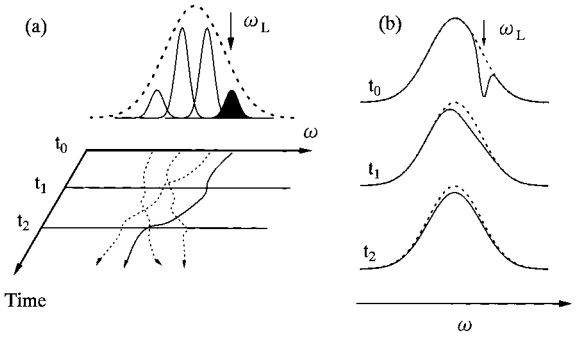

FIGURE 1: The schematic description of the TRTHB experiment. (a) The sharp spectrum (solid line) is the absorption spectrum of a single chromophore, and the broad spectrum (dashed line) is the ordinary absorption spectrum. Temporal fluctuation of the peak position of the single-chromophore spectrum is depicted in the lower part. (b) Temporal variation of the hole spectrum due to the spectral diffusion.

Here, one must note that the temporal change in the hole spectrum is induced essentially by the equilibrium conformational fluctuation process, but not by the relaxation from the nonequilibrium to equilibrium state (*19*). In a macroscopic sense, of course, the hole in the absorption spectrum is the nonequilibrium distribution, and the process in which the deformed spectrum recovers the equilibrium absorption spectrum should be called a relaxation. Here, however, one must recall that, in the TRTHB measurement, the temporal evolution of the hole is induced by the transition-energy fluctuation of the unexcited molecules that do not suffer from the perturbation by the exciting laser pulse and continue the equilibrium fluctuation even after the burning. Therefore, in a microscopic sense, the dynamics observed in the TRTHB measurement is controlled by the equilibrium fluctuation of the unexcited molecules. Therefore, we can strictly say that the dynamics observed by the TRTHB measurement is an equilibrium fluctuation. This is a conspicuous characteristic of this method as compared with those based on the flashphotolysis technique, in which the relaxation dynamics from the ligated to unligated state is observed. To the authors' knowledge, the TRTHB method is the only technique that offers the time-domain observation of the "equilibrium" fluctuation of a protein in a very wide temporal region, at present.

In a previous paper, comparison of the results between the ZnMb solution sample and the dye solution sample gave the evidence that the low-temperature protein dynamics is mainly controlled by the fluctuation of the solvent molecules (*19*). In the present article, we extend our studies further to the solvent effect on the protein dynamics. We have prepared ZnMb solution samples in 4 types of solvent conditions of known viscosity. We have also prepared one solid-state sample of ZnMb-doped polymer film. Then, the effect of the flexibility around the protein molecule has been systematically investigated.

Here, we are interested also in the influence of the energy landscape on the conformational dynamics of Mb. The time evolution of the hole spectrum has a close relationship to the shape of the energy landscape. If the CS's are hierarchi-

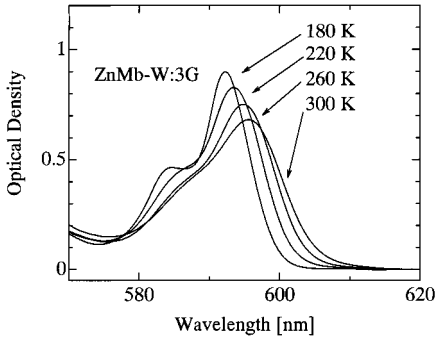

FIGURE 2: Temperature dependence of the absorption spectrum in the $Q(0,0)$ band region of ZnMb-W:3G.

cally arranged as widely accepted, the temporal shift of the hole may show a step-like time evolution; each step corresponds to the barrier-crossing process within one of the tiers. On the other hand, there also exist several studies which have shown that the simple harmonic-energy landscape well explains the experimental results (*21*−*23*). Agmon et al. have employed a simple model based on the assumption of the harmonic potential surface, and succeeded in reproducing the geminate recombination process of MbCO. In the present study, we employ this type of picture that assumes the harmonic potential surface. The observed temporal variation of the hole spectrum is analyzed on the basis of a treatment similar to that employed by Agmon et al., in which the conformational fluctuation is viewed as a Brownian motion within a harmonic potential surface. We introduce this simple model as a working hypothesis, although it contradicts the above mentioned idea of the hierarchical arrangement of CS's. We examine the validity of this analysis, and discuss the deviation of the observed data from this framework in relation to the shape of the energy landscape of Mb.

EXPERIMENTAL PROCEDURES

(A) Materials. The preparation of ZnMb was described in a previous paper (*24*). We prepared ZnMb samples in various matrices: in a buffered water−glycerol mixture with a glycerol volume ratio of 75% (ZnMb-W:3G), 50% (ZnMb-W:G), 0% (ZnMb-W), and in a buffered water−diglycerol mixture with a diglycerol volume ratio of 75% (ZnMb-W:3DG). The solvent viscosity at a given temperature increases in the order of W < W:G < W:3G < W:3DG. We also prepared ZnMb doped in a solid poly-vinyl-alcohol (PVA) film (ZnMb-PVA) with a thickness of about 0.5 mm. According to Austin et al. (*7*), we dissolved the solid PVA of 10% by weight in the same buffered water by boiling. After it was cooled to room temperature, the protein solution with the desired concentration was mixed and contained in a vessel, and then dried under Ar gas with a reduced pressure. After several days, a hard film was obtained. Phosphate buffer (10 mM) with pH 6.0 was used for all samples. The protein concentration was about 0.3 mM for the liquid samples and about 1 mM for the PVA film sample. Figure 2 shows the temperature dependence of the absorption spectrum of ZnMb-W:3G in the $Q(0,0)$ band region. All of the ZnMb samples have almost the same absorption spectrum as that in Figure 2, except for slight differences in the width and the peak position.

From the measurement of the far-UV circular dichroism (CD) spectrum of the sample, we confirmed that the secondary structure of Mb does not change so much by the Zn substitution and lowering of temperature (*19*). We also verified from the observation of the temperature dependence of the rotational relaxation time that a ZnMb molecule in a water−glycerol mixture maintains a rather compact tertiary structure in spite of the chromophore substitution (*25*). In fact, using a fluid mechanics model, we estimated the radius of a ZnMb molecule at ∼13 Å, which is even smaller than the value of 18.3 Å estimated from the X-ray diffraction data of Mb. In the case of ZnMb-PVA, the tertiary structure may be somewhat broken because the sample volume shrinks on the course of the drying process.

(B) Hole-Burning Measurements. Liquid samples were sealed in a glass cell with an optical path length of 2 mm. Both liquid and film samples were contained in a N_2 gas flow-type cryostat. The sample temperature was monitored by a thermocouple and maintained within ±0.5 K accuracy during the measurement. For ZnMb-W:G and ZnMb-W, we could not make experiments below the ice point because they became opaque at such a low temperature. Therefore, we made experiments for these samples at and above 280 K.

The hole was burned by using a dye laser (Lambda Physik SCANMATE rhodamine B) pumped by a frequency-doubled, Q-switched, diode-laser-seeded Nd:YAG laser (Spectra Physics GCR-130). The pulse duration was ∼7 ns, and the repetition rate was 10 Hz. The burning was made in the low-energy tail of the $Q(0,0)$ absorption band around 595 nm. For the probe light source, spontaneous emission from a dye solution pumped by another nanosecond laser was used. We employed a rhodamine 6G solution in ethanol with a concentration of ∼0.3 g/L for the emitting source. A dye cell containing the solution was pumped by second harmonic light of a Q-switched Nd:YLF laser (Spectra Physics TFR) with a pulse duration of ∼7 ns, and the dye solution emitted broad-band light with the spectrum ranging from 565 to 640 nm. The light transmitted through the sample was passed through a 25 cm single-grating polychromator (Oriel MS257) and detected with a CCD-camera system (Photometrics AT200) cooled by liquid nitrogen. The spectral resolution of the system was ∼2 Å. The wavelength calibration of this polychromator system was done by using the 632.8 nm line of a He-Ne laser and the sharp lines of Hg atoms sealed in a fluorescent lamp at 546.1, 579.1, and 577.0 nm.

The transient hole-burning spectrum at time t_d after the burning was obtained as

$$H(\omega, t_d) \equiv A'(\omega, t_d) - A(\omega) = -\log_{10}[\{I_{THB}(\omega, t_d) - I_{laser}(\omega)\}/I_{abs}(\omega)] \quad (2)$$

where $A(\omega)$ is the ordinary absorption spectrum before the burning, and $A'(\omega, t_d)$ is the absorption spectrum at t_d after the burning. I_{THB}, I_{laser}, and I_{abs} are the intensity of light transmitted through the sample under the irradiation of both burning and probing pulses, that under the burning pulse, and that under the probing pulse, respectively. Since the CCD camera used does not have a gating function, it was necessary to subtract I_{laser} in order to eliminate signal due to the scattered laser light and fluorescence from the sample.

Figure 3 shows a typical hole spectrum together with $A(\nu)$ and $A'(\nu)$ at 200 K. The hole spectrum is distorted around the burning wavenumber in spite of the subtraction of I_{laser} because of the fluctuation in the scattered light intensity.

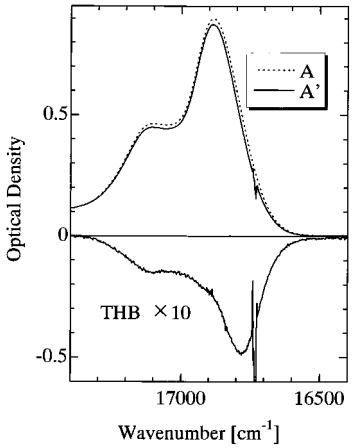

FIGURE 3: The typical THB spectrum (solid line) and the ordinary absorption spectrum before the burning, *A* (dashed line), and the absorption spectrum under the burning, *A′* (solid line), at 200 K. The latter spectrum is corrected by subtracting I_{laser}.

Although the difference between *A* and *A′* is very small, it is obvious that the hole is shifted from the position of the ordinary absorption spectrum to the low-energy side where the burning was made.

THEORETICAL BACKGROUND

(A) Expression for Time Evolution of THB Spectrum. In a previous paper (*26*), we already derived a phenomenological expression for the temporal change in the THB spectrum induced by the spectral diffusion depicted in Figure 1. Here, we briefly review this treatment. We express the absorption spectrum of a single chromophore as $a(\omega - \omega_0)$. Here, ω_0 is the angular frequency of the zero-phonon line, which corresponds to the purely electronic transition without excitation and deexcitation of the vibrational modes. ω_0 and $a(\omega - \omega_0)$ are called "site energy" and the single-site absorption spectrum of the chromophore, respectively. Here, we assume that each chromophore has the same single-site absorption profile but with a different site energy. Then, the ordinary absorption spectrum is expressed as

$$A(\omega) = \int a(\omega - \omega_0)G(\omega_0)\mathrm{d}\omega_0 \qquad (3)$$

where $G(\omega_0)$ denotes the distribution of the molecules which have the site energy at ω_0. The irradiation of the burning light pulse with frequency ω_L deforms the site-energy distribution function as

$$G'(\omega_0) = [1 - \phi a(\omega_L - \omega_0)]G(\omega_0) \qquad (4)$$

where ϕ is a constant proportional to the burning efficiency and the burning-pulse energy. Here, we assumed that the burning-pulse energy is so low that the saturation of the burning is negligible, and we neglected the de-excitation of the excited molecules due to stimulated emission. If the diffusive conformational motion of the apoprotein is not active, the shape of $G'(\omega_0)$ is independent of time after the burning. Then, the hole spectrum is expressed as

$$H(\omega;\omega_L) \equiv \int a(\omega - \omega_0)[G'(\omega_0) - G(\omega_0)]\mathrm{d}\omega_0 \propto -\int a(\omega - \omega_0)a(\omega_L - \omega_0)G(\omega_0)\mathrm{d}\omega_0 \qquad (5)$$

The diffusive conformational fluctuation of the protein induces the time dependence in the site-energy distribution of the chromophore. This spectral diffusion process can be treated by introducing a conditional probability $D(\omega_1,t;\omega_0)$, defined as the fraction of the chromophores with the site energy ω_1 at time t, when they initially have the site energy ω_0. The THB spectrum $H(\omega,t_d;\omega_L)$ at time t_d after the burning is expressed as

$$H(\omega,t_d;\omega_L) \propto -\int\int a(\omega - \omega_1)D(\omega_1,t_d;\omega_0) \times a(\omega_L - \omega_0)G(\omega_0)\mathrm{d}\omega_1\mathrm{d}\omega_0 \qquad (6)$$

(B) Configuration Coordinate Model. A configuration coordinate (CC) model with harmonic potential curves is one of the simplest models which can treat the time evolution of $D(\omega_1,t_d,\omega_0)$ (*20*, *27*). This model has successfully explained the effect of the solvation dynamics on the optical properties of dye solutions (*28*, *29*). Here, we derive the expression for the time evolution of *D* using the CC model in which the potential energy of the chromoprotein is assumed to be expressed by two parabolas as

$$U_g(Q) = aQ^2$$
$$U_e(Q) = a(Q - Q_0)^2 + \epsilon \qquad (7)$$

Here, U_g and U_e are the potential energies of the protein in the electronic ground and excited states of the chromophore, respectively. Of course, the energy landscape of protein is a function of a large number of coordinates of protein atoms, probably including the hydration shell. $U_g(Q)$ and $U_e(Q)$ are one-dimensional cross sections along the configuration coordinate *Q* which is responsible for the resonance-energy modulation of the chromophore. In this model, the effect of the barriers separating CS's is expressed as a friction on the potential surfaces. U_g and U_e are assumed to have the same curvature *a*, and to be shifted from each other by an amount Q_0. Since an optical transition occurs between the states with the same value of *Q*, the resonance energy of the chromophore depends linearly on *Q*. Thus, the site-energy ω_0 of the chromophore is expressed as

$$\hbar\omega_0(Q) = U_e(Q) - U_g(Q) = -2aQ_0Q + aQ_0^2 + \epsilon \qquad (8)$$

where $\hbar$ is the Plank's constant divided by 2π.

According to van der Zwan and Hynes (*27*) and Kinoshita (*20*), we treat the motion of *Q* as a Brownian diffusion in a harmonic potential of U_g. Then, the fluctuation of *Q* can be regarded as a Gaussian random process, and we obtain the expression for the time evolution of *D* as

$$D(\omega_1,t;\omega_0) = \frac{1}{\sqrt{2\pi\langle\Delta\omega_0^2\rangle(1 - C^2(t))}}\exp\left[-\frac{(\Delta\omega_1 - \Delta\omega_0 C(t))^2}{2\langle\Delta\omega_0^2\rangle(1 - C^2(t))}\right] \qquad (9)$$

with

$$C(\tau) \equiv \langle Q(t)Q(t+\tau)\rangle/\langle Q^2\rangle$$
$$\Delta\omega_{0/1} = \omega_{0/1} - \langle\omega_0\rangle$$

$$\langle \omega_0 \rangle = \frac{aQ_0^2 + \epsilon}{\hbar}$$

$$\langle \Delta\omega_0^2 \rangle \equiv \langle (\omega_0 - \langle \omega_0 \rangle)^2 \rangle = \frac{2aQ_0^2 k_B T}{\hbar^2} \qquad (10)$$

Here, $C(\tau)$ is the normalized correlation function and $\langle\ \rangle$ denotes the ensemble average. $\langle \omega_0 \rangle$ and $\langle \Delta\omega_0^2 \rangle$ correspond respectively to the peak position and dispersion of the site-energy distribution function having the form of

$$G(\omega_0) = \lim_{t \to \infty} D(\omega_0, t; \omega') = \frac{1}{\sqrt{2\pi\langle \Delta\omega_0^2 \rangle}} \exp\left[-\frac{\Delta\omega_0^2}{2\langle \Delta\omega_0^2 \rangle} \right] \qquad (11)$$

Equations 6, 9, and 11 predict an symptotic behavior of the hole spectrum burned in the absorption spectrum; its peak position and spectral width approach those of the ordinary absorption spectrum with increasing t_d, and its shape becomes equal to that of the absorption spectrum in the limit of $t_d \rightarrow \infty$. Here, we should point out that the above prediction that the hole profile in the limit of $t_d \rightarrow \infty$ coincides with the absorption profile is valid regardless of the model employed. The energy landscape other than the harmonic shape may result in a more complicated temporal evolution of the hole profile than the case of the harmonic one. In such a case, nonetheless, the hole shape becomes equal to the absorption shape when the deformed site-energy distribution recovers the thermal equilibrium. Equations 10 and 11 also predict that the width of the site-energy distribution function $G(\omega_0)$ is proportional to $\sqrt{T}$, which is roughly consistent with the observed temperature dependence of the absorption spectrum shown in Figure 2. This suggests that the Boltzmann distribution is established in the ground state at a temperature higher than 180 K.

Our treatment presented above is similar to that employed by Agmon et al. Probably for simplicity, in their formalism the conformational dynamics has been assumed to obey the Smoluchowski equation, which leads to a time-correlation function with the single-exponential time dependence (*22, 23*). On the other hand, the present model is available not only for a single-exponential correlation function but also for an arbitrary type of correlation function. As it will be shown later, this generalized formalism is important to analyze the experimental results of ZnMb.

RESULTS AND ANALYSIS

(A) Temporal Variation of THB Profile. The primary aim of the present experiment is to detect the temporal change in the hole profile induced by the conformational fluctuation of a Mb molecule. In the nanosecond to millisecond time region, however, the hole profile is affected also by the rotational diffusion process of the protein molecule as well as by the conformational fluctuation. To eliminate the rotational effect, we measured the hole spectrum in the "magic angle" configuration, in which the angle θ between the polarizations of the probe and burning beams satisfies the relation $\sin^2\theta = 2\cos^2\theta$. Further, we took care that the hole depth does not exceed 10% of the ordinary absorbance

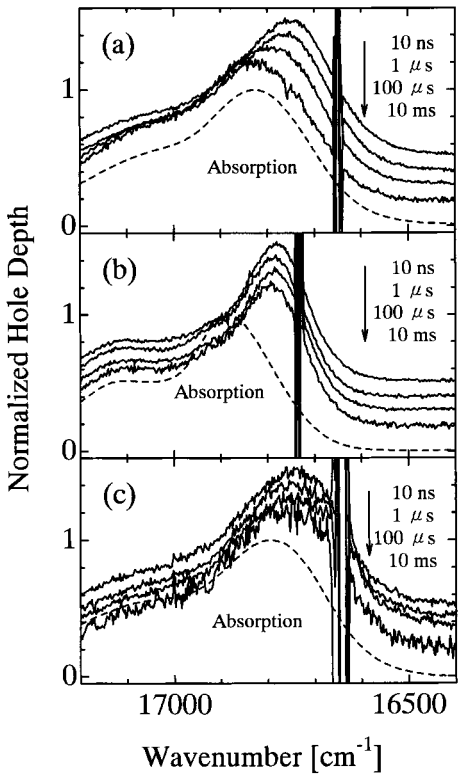

FIGURE 4: Time evolution of the normalized TRTHB spectra of ZnMb-W:3G at 240 K (a) and 180 K (b), and of ZnMb-PVA at 240 K (c). The spectra are offset vertically to avoid overlap. The dashed lines denote the normalized absorption spectra. The excitation wavenumber is 16 653 cm^{-1} for (a) and (c), and 16 736 cm^{-1} for (b).

so that the saturation effect does not distort the hole shape. The employed burning-power density was ~1 mJ/cm^2, and the resulting difference in the optical density was about 0.05. To cause a large temporal shift of the THB spectrum, we burned a hole in the low-energy tail of the $Q(0,0)$ absorption band. We chose the burning wavelength so that the optical density of the sample at the burning wavelength is 20−30% of the absorption maximum. Since ZnMb shows marked temperature dependence of the peak energy of the absorption spectrum as shown in Figure 2, we carefully adjusted the burning wavelength at each temperature.

Figure 4 shows the temporal variation of the THB spectra of ZnMb samples (solid lines) together with the ordinary absorption spectra for the same sample conditions (dashed lines). Both the depth of the THB spectrum and the height of the absorption spectrum are normalized to unity for comparison. Spikes around the burning wavenumber in the hole spectra are due to the scattering of the burning laser light. In Figure 4a, the main peak of the THB spectrum moves from 16 750 to 16 820 cm^{-1} (by about 70 cm^{-1}) for ZnMb-W:3G at 240 K as the delay time of the probe pulse after the burning is prolonged from 10 ns to 10 ms. Time-dependent broadening of the hole width was also observed although it is not clear in Figure 4a. These temporal changes in the hole profile are caused by the conformational fluctuation of the ZnMb molecules which were not selected by the burning. The hole spectrum has a sideband in the high-energy region around 17 100 cm^{-1}, which appears also in the ordinary absorption spectrum at low temperatures as shown in Figure 2. From the analysis of the polarization dependence

of the THB spectra, we showed that this sideband corresponds to the absorption into a higher-energy excited state, whose transition dipole is perpendicular to that of the main band (*30*). This sideband shows little time-dependent shift at all temperatures examined, probably because a very broad homogeneous width of this band smears its temporal change.

In the case of ZnMb-W:3G at 180 K (Figure 4b), the hole spectrum remains at the initial position regardless of the delay time. This clearly indicates that the diffusive conformational fluctuation in the 10 ns to 10 ms time scale is frozen out in Mb at 180 K. It is also noticed in Figure 4b that the hole width is much smaller than that observed at 240 K. The hole width just after the burning is caused by the fluctuation process faster than the experimental time resolution of 10 ns. It is considered that the vibrational motion gives a dominant contribution to the hole broadening just after the burning (*25, 26*), and then the smaller hole width observed at 180 K can be attributed mainly to the diminution of the vibrational motion by lowering temperature. In Figure 4c, we show the time evolution of the THB spectrum of ZnMb-PVA at 240 K. Since the laser scattering from the sample surface is very strong for the PVA film sample, the observed THB spectra are considerably distorted. Nevertheless, Figure 4c clearly shows that the peak position of the hole of ZnMb-PVA hardly changes with increasing delay time, while the hole spectrum has a width comparable to that for ZnMb-W:3G at 240 K. Hence, it is suggested that, if a Mb molecule is doped in a solid matrix, the diffusive conformational motion is suppressed, while the vibrational motion inducing the hole broadening just after the burning is still active.

To analyze the temporal change in the hole profile, we introduce the time-dependent first moment $c(t_d)$ and the dispersion $\sigma^2(t_d)$ of the THB spectrum as

$$c(t_d) \equiv \langle\omega(t_d)\rangle_{THB} - \langle\omega\rangle_{abs} = \frac{\int_{\omega_1}^{\omega_2} \omega H(\omega, t_d)d\omega}{\int_{\omega_1}^{\omega_2} H(\omega, t_d)d\omega} - \frac{\int_{\omega_1}^{\omega_2} \omega A(\omega)d\omega}{\int_{\omega_1}^{\omega_2} A(\omega)d\omega} \quad (12)$$

$$\sigma^2(t_d) \equiv \frac{\int_{\omega_1}^{\omega_2} (\omega - \langle\omega(t_d)\rangle_{THB})^2 H(\omega, t_d)d\omega}{\int_{\omega_1}^{\omega_2} H(\omega, t_d)d\omega} \quad (13)$$

As seen in eqs 6, 9, and 11, when the site-energy distribution deformed by the burning recovers the equilibrium distribution, the shape of the THB spectrum agrees with that of the absorption spectrum. Then, it is expected that, in the limit of $t_d \rightarrow \infty$, $c(t_d)$ tends to 0 and $\sigma^2(t_d)$ becomes equal to the dispersion of the absorption spectrum. To reduce the influence of the drift in the tail region of the spectrum, we calculated the above functions by integrating the observed spectra over a limited wavenumber range between ω_1 and ω_2. For all the spectra, we selected the energy positions where the height of the spectrum is 20% and 80% of its maximum as the low- (ω_1) and high- (ω_2) energy limits of the calculation, respectively. Thus, we excluded the sideband around 17 100 cm^{-1} from the calculation. Furthermore, we eliminated the distortions due to the laser scattering in the observed THB spectra by replacing the spectrum around the laser wavenumber by an appropriate quadratic function.

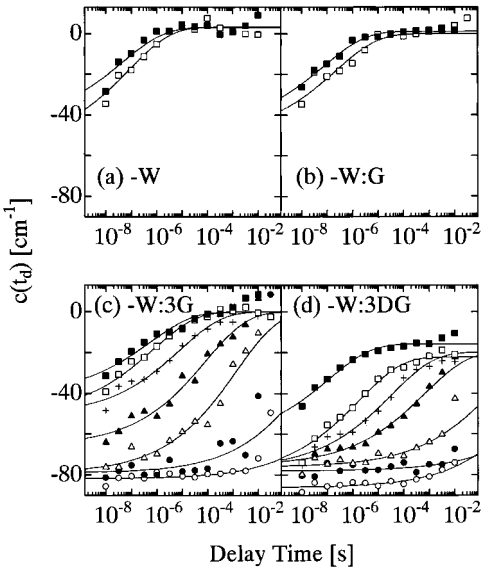

FIGURE 5: The time evolution of $c(t_d)$ for ZnMb-W (a), ZnMb-W:G (b), ZnMb-W:3G (c), and ZnMb-W:3DG (d) at 180 K (○), 200 K (●), 220 K (△), 240 K (▲), 260 K (+), 280 K (□), and 300 K (■). The solid lines are the fitting curves to eq 14 obtained by the least-squares method.

In Figure 5, we compare the temporal evolution of $c(t_d)$ for ZnMb solution samples at various temperatures. The solid lines are the fitting curves discussed later. For all samples, $c(t_d)$ at moderate temperatures show highly nonexponential t_d dependence over a time range 10 ns to 1 ms, and the time scale of the change in $c(t_d)$ becomes faster with increasing temperature. The temporal change in the THB spectrum in the time region $t_d > 1$ ms is not reliable, because the accumulated population in the T_1 state begins to relax to the ground state in this time region and this hole-filling process may affect the hole spectrum. Hence, it is difficult to determine whether the temporal change observed in $c(t_d)$ for $t_d > 1$ ms is due to the conformational fluctuations in the ground state or in the excited state. Anyway, we can say from Figures 5c,d that the suppression of the conformational fluctuation of ZnMb by lowering temperature occurs around 180 K for ZnMb-W:3G and 200 K for ZnMb-W:3DG. These results are consistent with the interpretation that the glass-like transition of Mb occurs around 200 K (*3, 14, 15*). On the other hand, comparison of the results between ZnMb-W:3G and ZnMb-W:3DG indicates that the conformational dynamics observed in the present TRTHB study depends on the solvent condition. This becomes more evident in Figure 6, which clearly shows that $c(t_d)$ for ZnMb-PVA is almost time-independent at all temperatures examined. This confirms that the diffusive conformational motion of Mb is no longer active if it is surrounded with a solid matrix.

In Figure 7, we show the temporal evolution of $\sigma^2(t_d)$ for ZnMb solution samples. Probably because the calculation of $\sigma^2(t_d)$ is more sensitive to the drift of the data, $\sigma^2(t_d)$ obtained is scattered more than $c(t_d)$. However, Figure 7 still indicates that the time-dependent hole broadening occurs in approximately the same time region as that in $c(t_d)$. It is found that $\sigma^2(t_d)$ shows an asymptotic approach to the dispersion of the absorption spectrum with increasing delay time.

(B) Analysis by CC Model. Equations 6 and 9 predict that the time characteristics of $c(t_d)$ and $\sigma^2(t_d)$ are proportional to $C(t_d)$ and $1 - C^2(t_d)$, respectively. Thus, in the CC model,

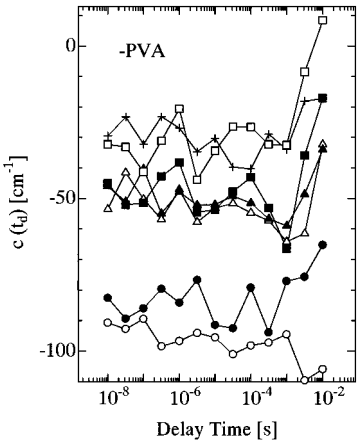

FIGURE 6: The time evolution of $c(t_d)$ for ZnMb-PVA. The meanings of the symbols are the same as in Figure 5. The data points at the same temperature are linked to each other by solid lines for guides of eyes.

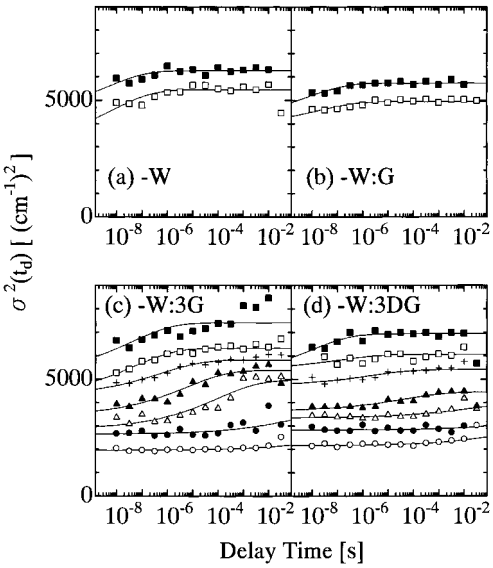

FIGURE 7: The time evolution of $\sigma^2(t_d)$ for ZnMb-W (a), ZnMb-W:G (b), ZnMb-W:3G (c), and ZnMb-W:3DG (d). The meanings of the symbols are the same as in Figure 4. The solid lines are the fitting curves to eq 16 obtained by using the same value for τ_c and β as those determined in the fitting of $c(t_d)$.

both the temporal shift and broadening of the hole can be expressed by using the same normalized correlation function, $C(t_d)$. We fitted the obtained $c(t_d)$ for solution samples to an empirical expression of a stretched exponential form, $\exp[-(t_d/\tau_c)^\beta]$ with $0 < \beta < 1$, which has been known to reproduce nonexponential relaxation observed in a great variety of glasses and in proteins (*3, 31, 32*). The solid lines in Figure 5 are the fitting curves expressed as

$$c(t_d) = A_c + B_c \exp[-(t_d/\tau_c)^\beta] \qquad (14)$$

where A_c and B_c are the parameters adjusting the value at $t_d \gg \tau_c$ and the amount of the time-dependent shift of $c(t_d)$, respectively. The CC model predicts that the hole profile at $t_d \gg \tau_c$ agrees with the ordinary absorption spectrum, and then $A_c = 0$. However, this is not the case if the triplet-triplet absorption spectrum due to the transition of the chromophores accumulated in the lowest triplet state into a higher triplet state overlaps the hole spectrum. Therefore,

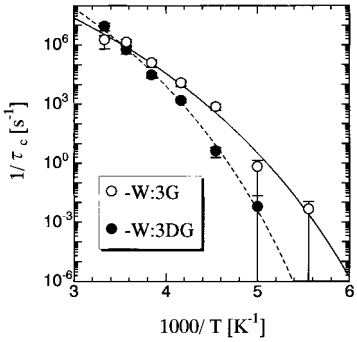

FIGURE 8: The temperature dependence of $1/\tau_c$ determined for ZnMb-W:3G (○) and ZnMb-W:3DG (●). The solid and dashed lines are the fitting curves to the Vogel−Fulcher law expressed by eq 17.

the parameter A_c is necessary to fit the observed $c(t_d)$ adequately.

All 4 parameters of A_c, B_c, τ_c, and β can not be determined simultaneously by the least mean-square fitting at low (<220 K) and high (>260 K) temperatures, because only a part of the temporal change in $c(t_d)$ is observed within the experimental time window in these temperature regions. In the fitting procedure, therefore, first we fitted the data in the intermediate temperature range of 220−260 K for ZnMb-W:3G and 240−260 K for ZnMb-W:3DG, where the whole temporal change in $c(t_d)$ is observed. In this prefitting, we took B_c, τ_c, and β as free parameters, and A_c was fixed at 0 and −20, respectively, for ZnMb-W:3G and ZnMb-W:3DG, which are rough asymptotic values of $c(t_d)$ for $t_d \rightarrow \infty$ above 260 K. Then, we averaged the values of β determined by this prefitting and obtained the value 0.26. This is slightly larger than the value 0.22 reported in the previous paper (*19*). This slight discrepancy arises because the value 0.22 was obtained by considering only the data for ZnMb-W:3G, while the present value of 0.26 was determined from the data for both ZnMb-W:3G and ZnMb-W:3DG. The value of 0.26 is still much smaller than ∼0.5 that has been usually obtained in the relaxation process of various glass formers (*31*). For a correct estimation of the value of τ_c, we refitted all the data for ZnMb solution samples with β fixed at the averaged value 0.26. Thus, here we assumed the validity of the time−temperature scaling principle for $c(t_d)$, so that $c(t_d)$ obtained at different temperatures fall on a single master curve with different τ_c. The data points of $c(t_d)$ for $t_d \geq 10$ ms were neglected in the fitting because they may be affected by the hole-filling effect. The solid lines in Figure 5 are thus obtained fitting curves, which reproduce the observed data well. By using eqs 9 and 14, we can estimate an approximate shape of the normalized correlation function of Q as

$$C(t_d) \approx \frac{c(t_d) - A_c}{c(t_d \rightarrow 0) - A_c} \approx \exp[-(t_d/\tau_c)^\beta] \qquad (15)$$

Therefore, the obtained τ_c turns out to be the correlation time of the fluctuation process of Q in the framework of the CC model. Here, we do not call τ_c as the relaxation time but as the correlation time in order to emphasize that the observed temporal change in the hole spectrum is essentially induced by the equilibrium fluctuation process, but not by the nonequilibrium relaxation process.

Next, we discuss the temporal evolution of the hole width. According to eqs 9 and 15, we obtain an approximate relation

$$\sigma^2(t_d) \approx A_\sigma + B_\sigma\{1 - C^2(t_d)\} \approx A_\sigma + B_\sigma\{1 - \exp[-2(t_d/\tau_c)^\beta]\} \quad (16)$$

where A_σ and B_σ are the parameters adjusting the initial value and the amount of the time-dependent increase in $\sigma^2(t_d)$, respectively. The solid lines in Figure 7 are the fitting curves of the observed $\sigma^2(t_d)$ to eq 16. In this fitting, we used the values of τ_c and β (= 0.26) determined in the fitting of $c(t_d)$, and took the remaining parameters A_σ and B_σ free to vary. The fitting curves reproduce the observed $\sigma^2(t_d)$ fairly well. The value of $A_\sigma + B_\sigma$ determined in the fitting is approximately equal to the dispersion of the ordinary absorption spectrum, which is consistent with the prediction of the CC model. Hence, we can say that the temporal change in both the peak position and width of the THB spectrum can be reproduced on the basis of the CC model. This suggests that the model in which the conformational fluctuation of Mb is viewed as a Brownian motion in a harmonic potential gives a rather good description of the actual situations.

(C) Temperature and Viscosity Dependence of Correlation Time. We plot the temperature dependence of $1/\tau_c$ obtained for ZnMb-W:3G (○) and ZnMb-W:3DG (●) in Figure 8. The data points slower than 1 s have large error bars and are not reliable, because the temporal window of the measurement does not cover such a long delay-time region. In spite of this uncertainty, it is clear that the temperature dependence of τ_c is well reproduced by the Vogel−Fulcher formula

$$\tau_c = \tau_0 \exp[E/(T - T_0)] \quad (17)$$

which is known to hold in various glassy materials, rather than the simple Arrhenius law. The solid and dashed lines in Figure 8 are the fitting curves of the data for ZnMb-W:3G and ZnMb-W:3DG to eq 17, respectively. The determined parameters are $\tau_0 = 5.44 \times 10^{-13}$ s, $E = 2573$ K, and $T_0 = 105$ K for ZnMb-W:3G, and $\tau_0 = 9.72 \times 10^{-15}$ s, $E = 3013$ K, and $T_0 = 120$ K for ZnMb-W:3DG. The simulated curves well fit the observed temperature dependence of $1/\tau_c$. Figure 8 clearly indicates that ZnMb-W:3DG shows stronger temperature dependence of $1/\tau_c$ than ZnMb-W:3G, while they have a similar value of τ_c at room temperature. Thus, it is obvious in Figure 8 that the diffusive conformational motions of ZnMb-W:3DG slow down more readily by lowering the temperature than those of ZnMb-W:3G.

Next, we discuss the dependence of $1/\tau_c$ on the solvent viscosity η shown in Figure 9. As the temperature dependence of η of the water−glycerol mixtures, we employed the well-known Hasinoff's empirical law (*33*) which is warrantable above 230 K. That of the pure water was quoted from a typical handbook of chemistry and physics. On the other hand, we measured the viscosity of the water−diglycerol mixture at and above 220 K by using a cryogenic rheometer (Rheometric Scientific FE ARES-2KFRT). In Table 1, the temperature dependence of η of the solvent used in the experiment is summarized. The solid line in Figure 9 is a fitting curve to a linear function

$$\tau_c = \frac{\eta + \sigma}{A} \quad (18)$$

with $A = 1.26 \times 10^8$ [cP/s] and $\sigma = 7.46$ [cP]. The fitting curve agrees well with the obtained data. Thus, Figure 9 shows that τ_c is linearly dependent on the solvent viscosity regardless of the solvent composition and temperature. Here, it is noticeable that the exponential term in eq 1 is no longer necessary in a very wide viscosity region in the present case. Thus, it is suggested that τ_c depends on T only indirectly through the T dependence of η, and that the solvent viscosity rather than temperature plays a crucial role in determining the dynamics of Mb observed here.

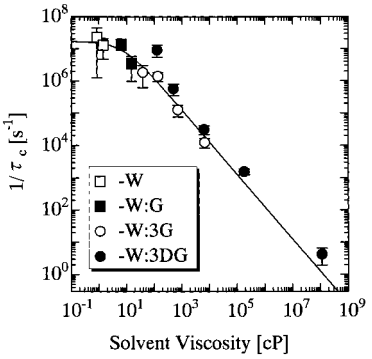

FIGURE 9: The solvent viscosity dependence of $1/\tau_c$ determined for ZnMb-W (□), ZnMb-W:G (■), ZnMb-W:3G (○), and ZnMb-W:3DG (●). The solid line is the fitting curve to a linear function of the solvent viscosity given by eq 18.

Table 1: Viscosity [cP] of the Water−Glycerol and Water−Diglycerol Mixtures as a Function of Temperature

solvent condition	220 K	240 K	260 K	280 K	300 K
W				1.43	8.51×10^{-1}
W:G				1.50×10^1	6.40
W:3G		6.66×10^3	7.15×10^2	1.35×10^2	3.83×10^1
W:3DG	1.14×10^8	1.82×10^5	6.40×10^3	4.98×10^2	1.26×10^2

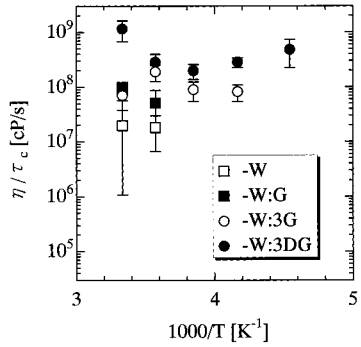

FIGURE 10: The temperature dependence of η/τ_c determined for ZnMb-W (□), ZnMb-W:G (■), ZnMb-W:3G (○), and ZnMb-W:3DG (●).

This becomes more legible in Figure 10, in which the correlation time scaled by the solvent viscosity is plotted as a function of the inverse of T. If $1/\tau_c = k$ obeys eq 1, $1/T$ dependence of $\log(\eta/\tau_c)$ will show a negative slope in the low-temperature region, which corresponds to $-H/k_B$. In Figure 10, however, $\log(\eta/\tau_c)$ is almost temperature-independent, or even decreases with increasing temperature reflecting the saturation of $1/\tau_c$ in the low-viscosity region. This verifies that H in eq 1 is very small or essentially 0 in the present case.

DISCUSSION

(A) Characterization of Energy Landscape. The hierarchical arrangement of CS's of Mb has been established by

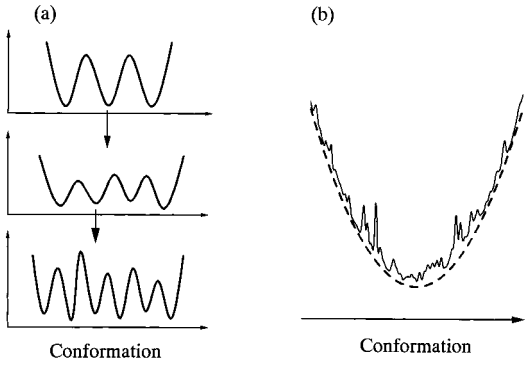

FIGURE 11: The energy landscape of Mb. (a) The hierarchical arrangement of CS's. (b) Harmonic potential with the hierarchical CS's on its surface.

various experiments such as the band III relaxation measurements (*2, 4*). The most compelling evidence for the hierarchical CS's comes from the infrared (*14*) and resonance-Raman (*34*) spectroscopic studies on the stretching band of MbCO, which have clarified that it consists of three or four bands, implying that MbCO can exist in three or four conformations, that is, in the so-called A_0-A_3 substates. These substates have been considered to belong to the highest tier of the hierarchy. The interconversion rates among these *A* substates have been estimated by a double-pulse flash-photolysis experiment (*12*) and a pressure-release experiment (*35*). On the basis of these experimental results, the energy landscape depicted in Figure 11a has been proposed (*2*).

The hierarchical arrangement of CS's mentioned above should affect the time evolution of both $c(t_d)$ and $\sigma(t_d)$ observed in the present study. The energy landscape drawn in Figure 11a will result in a discrete distribution of the barrier height separating CS's. Then, crossing of the barriers belonging to different tiers may take clearly different times. If plotted versus $\log(t_d)$, $c(t_d)$ and $\sigma(t_d)$ consequently may show time evolution with discrete phases; each phase corresponds to the fluctuation process in different tiers. As described in Results and Analysis, in contrast, the observed $c(t_d)$ and $\sigma(t_d)$ were reproduced well by a stretched exponential function with a single time constant. In addition, the whole observed data were reproduced rather well on the basis of a simple harmonic potential model discussed in Theoretical Background. This implies that the overall profile of the energy landscape is expressed fairly well by a parabolic function, rather than the shape depicted in Figure 11a. However, a close look at Figure 5c,d may suggest that the data points for both ZnMb-W:3G and ZnMb-W:3DG at 240 K (△) and 260 K (+) can be fitted to a sum of two exponential functions, as well as to a single stretched-exponential function. It is possibly a sign of the discrete barrier height distribution predicted by the hierarchical CS's. In spite of this sign, it can be said that, in this relatively high temperature region, the effect of the discrete barrier-height distribution is rather small, resulting in the nearly single-phase behavior of $c(t_d)$ as shown in Figure 5. To confirm this effect, the investigation of the more detailed shape of $c(t_d)$ is one of the important future problems.

There is another observable which gives information about the shape of the energy landscape. As shown in eq 11, the assumption of the harmonic potential surface leads to a site-energy distribution function $G(\omega_0)$ with a Gaussian shape. Thus, the deviation of the site-energy distribution function from a Gaussian shape can be an indicator of unharmonicity of the potential surface. So far, Kaposi et al. (*36*) and Ahn et al. (*37*) have independently succeeded in determining the precise shape of $G(\omega_0)$ respectively for Mg-substituted Mb (MgMb) and ZnMb, by using the fluorescence line-narrowing technique at a cryogenic temperature. Their results have shown that the shape of $G(\omega_0)$ somewhat deviates from a Gaussian shape (especially for MgMb but not so much for ZnMb) at a cryogenic temperature. This clearly indicates that the potential surface is not completely harmonic at least at cryogenic temperatures. The above-mentioned step-like behavior of $c(t_d)$ at 240 and 260 K may be related to the unharmonicity of the potential surface thus inferred from the shape of the low-temperature $G(\omega_0)$. At a higher temperatures, however, the deviation of $G(\omega_0)$ from a Gaussian shape seems small so that the absorption spectrum above ~200 K can be approximated by a Gaussian shape (see Figure 2). Probably, the effective potential surface is roughly expressed by a parabola at higher temperatures.

The value of β also has a close relation to the shape of the energy landscape. As shown in Figure 5, the assumption of the temperature-independent β seems to hold, suggesting the validity of the time−temperature scaling principle of the correlation function. The average value of β of 0.26 is considerably small compared with those usually estimated around 0.5 in the relaxation process of various disordered systems (*31*). In fact, in the TRTHB studies of dye-doped viscous solvents, β, was determined to be ~0.5 (*19, 38*). The remarkably small β of ZnMb solutions indicates a wider distribution of the fluctuation time scale. At a first glance, small β, or a very wide distribution of the time scale, appears to imply a more disordered characteristic of ZnMb than the ordinary glass former, and to contradict the established idea that the protein has a more ordered structure than the ordinary glasses. We interpret the origin of the small β as follows. The stretched exponential correlation function of the conformational fluctuation is due to the interaction among various steps of motions of groups of atoms with different sizes. The cooperative nature of the fluctuation process makes the correlation function nonexponential (*31, 39*). Namely, the motion of an atomic group with a larger size can not occur unless the appropriate configuration of atoms is achieved through the rearrangement of atomic groups with smaller sizes. The small β estimated for a protein is, therefore, interpreted in terms that the molecular motions in a very wide variety of classes simultaneously participate in a protein solution. The smallest step may be a motion of the surrounding solvent molecules, and the largest step may be a rearrangement of the domain unit which is absent in ordinary glasses.

Anyway, owing to this small β, a ZnMb molecule shows a very slow conformational fluctuation process in the microsecond region even in physiological conditions. In other words, it takes about a few microseconds for a ZnMb molecule to walk around all the energetically allowed phase space even at room temperature. In most molecular dynamics (MD) simulations, on the other hand, the typical sampling time is at most a few nanoseconds, which is far shorter than the equilibration time estimated here. Therefore, one must take care in comparing the results of such simulations and the experimental results which are obtained as the ensemble

average over the thermal equilibrium distribution. Of course, the equilibration time will be different for different proteins. In fact, our recent experiment on Zn-substituted cytochrome c indicates that it has a somewhat shorter equilibration time than ZnMb (see the following article).

According to the above discussion, we introduce in Figure 11b a picture of the energy landscape of ZnMb which adequately accounts for the tendency of the observed data. Its overall shape, that is, the envelope on which many local minimums are located, is expressed by a parabolic function (dashed line). The heights of the potential barriers separating the local minimums form a rather continuous distribution, while in Figure 11a, three distinct conformers exist in the highest tier of the hierarchical CS's. The inconsistent conclusions obtained from our experiment and the above-mentioned vibrational spectroscopy might arise from the different dynamical character between ZnMb and the intact Mb. However, it is more probable that these inconsistent results come from the difference in the probe used. In the vibrational spectroscopy, the probe of the conformational change in the apoprotein is the frequency of the CO-stretching mode. This is a very small probe as compared with the Zn-protoporphyrin molecule used in the present experiment. Such a small probe may be much more sensitive to a local conformational difference, rather than to the difference in the global conformation. In the vibrational measurements, therefore, the proximate conformation around the CO molecule is reflected more strongly on the experimental results than the global conformation. In the present TRTHB case, on the other hand, a much larger molecular probe is employed, and the information about the local conformation may be filtered out and that about the global conformation is mainly obtained. We believe that a Mb molecule in this temperature region feels the potential surface as shown in Figure 11b.

Here, we must point out that what are shown in Figure 11 are the energy landscapes of ZnMb defined as functions of the degrees of freedom of both the protein and the solvent molecules interacting with the protein. Kitao et al. compared the trajectory of the MD simulation of melittin in water with that in vacuum (*40*). The MD trajectory in water shows a very diffusive character associated with transitions from one conformation to another, while that in vacuum displays a smooth, oscillative motion. They concluded that the diffusive character of the MD trajectory in water results from the interaction between melittin and the first- and the second-shell hydrated water molecules (*41*, *42*). Their analysis clearly indicates that the roughness of the potential surface of a protein comes partly from the solvent molecules imposing constraint on the conformational dynamics of a protein. Hence, the degrees of freedom of the surrounding solvent can no longer be ignored to account for the dynamical character of the protein conformation. We, therefore, introduced the energy landscape as a function of both the protein conformation and surrounding solvent configuration. Crossing of the lowest barrier in Figure 11 may correspond to the change in the solvent configuration. The following discussion is based on this idea.

(B) Solvent Effect in Terms of Hierarchically Constrained Dynamics Model. Figure 9 clearly shows that the solvent viscosity influences critically the conformational dynamics of ZnMb especially in the high-viscosity region. This again shows that the observed process corresponds to a rather global conformational motion involving the motions of the residues having direct contacts with the solvent molecules. This thought is also supported by the fact that ZnMb doped in a solid polymer matrix exhibits no diffusive conformational motion. In Figure 10, it is obvious that H in eq 1 is very small or almost 0, suggesting that the temperature plays only a secondary role in determining the conformational dynamics of a Mb molecule in high-viscosity region. This gives a crucial evidence for the solvent-induced glass-like transition of Mb around 200 K. Although it is still a controversial problem whether the glass-like transition of a protein is induced by the solvent, we believe from the above result that the quenching of the fluctuation by lowering temperature is induced by the freezing of the solvent, at least in the case of Mb. In the low-viscosity region, on the other hand, τ_c appears to become less sensitive to η. From the fitting curve in Figure 9, τ_c in the limit of $\eta \rightarrow 0$ can be roughly estimated at 5.9×10^{-8} s. As pointed out by Ansari et al. (*9*), this saturation of $1/\tau_c$ may reflect the fact that the internal friction in the protein becomes effective in such a low-viscosity region of physiological importance.

The linear dependence of τ_c on η shown in Figure 9 can not be understood by simply assuming the Arrhenius-type crossing of the barriers on the potential energy surface of Figure 11b. This is because the assumption of such a barrier-crossing process results in the temperature dependence of τ_c predicted by eq 1 with H of a non-zero value, which is not the case in the present experiment. Hence, we must explain simultaneously the two phenomena in Mb solutions; one is the stretched-exponential behavior of $C(t_d)$ with a small, almost temperature-independent β, and the other is the linear η dependence of τ_c without any apparent temperature dependence.

There exists a simple model, the hierarchically constrained dynamics (HCD) model proposed by Palmer et al. (*39*), which explains adequately the former phenomenon. In this model, the degrees of freedom of the system are represented by N Ising spins, each of which belongs to one of many hierarchical levels, $n = 0, 1, 2, \ldots$. There are N_n Ising spins in the level n. Then, it is assumed that the dynamics in a lower level imposes constraint on the dynamics in a higher level. This constraint is expressed by the condition that each spin in level $n + 1$ can flip only when a certain condition on μ_n ($\mu_n \leq N_n$) spins in level n is satisfied. With these postulates, the correlation function is obtained as

$$C(t) = \sum_{n=0}^{\infty} (N_n/N)\exp(-t/\tau_n) \tag{19}$$

with the relation

$$\tau_{n+1} = 2^{\mu_n}\tau_n \tag{20}$$

Here, τ_n is the average correlation time of the spins in level n. Because of the flexibility of this model, various types of $C(t)$ can be realized by arbitrarily assuming how N_n and μ_n depend on n, in principle. In fact, with the relations $\mu_n = \mu_0 n^{-p}$ with $p \geq 1$ and $N_n = N_0/\lambda^n$, Palmer et al. succeeded in reproducing the stretched-exponential $C(t)$. Here, however, we do not introduce any concrete relation for μ_n and N_n, because this model probably oversimplifies the real situation,

and also because the parameters p or λ will have few meanings. Nevertheless, this model reproduces the important aspect, that is, the time−temperature scaling principle, if n dependence of both μ_n and N_n is not temperature-dependent. According to this HCD model, hence, we can give a qualitative explanation for the stretched exponential behavior of $C(t_d)$ with the temperature-independent β. In this case, the temperature dependence of $C(t)$ is attributed to that of τ_0, the average correlation time of the spins in the lowest level.

We can show that the linear η dependence of τ_c is also understood qualitatively based on the HCD model with the following postulates. The flips of the spins in the lowest level in the HCD model correspond in the real system to the motions of the solvent molecules surrounding the protein, and η depends linearly on the solvation relaxation time. The latter assumption may be reasonable because η is known to be proportional to the shear-stress relaxation time (*31*). The idea that the different configuration of the solvation shell around the protein gives different relaxation times of protein has been also presented and discussed by Huang et al. (*11*). Although this notion is no more than a speculation, it sounds quite convincing especially if we take into account the results of the following investigations. It has been found from the MD simulation that the change in the packing topology of the surrounding solvent molecules plays an important role in the conformational transition of the solute molecule (*41, 42*). Furthermore, in their simulation, the rotational relaxation time of the hydrated molecules has been estimated at 3−4 ps, which approximately lies in the initial stage of the temporal change in $C(t)$ for ZnMb-W at 300 K.

In this framework, therefore, the linear η dependence of τ_c is attributed to the linear relation between η and τ_0 which is also proportional to τ_c in the HCD model. Thus, we can give a qualitative explanation of the η dependence of τ_c based on the HCD model. The saturation behavior of $1/\tau_c$ in the low-viscosity region can also be understood in this framework. While the motions of the solvent molecules become faster with lowering viscosity, the conformational motion of a protein can not become infinitely fast because of the internal constraint in the protein. Then, in the low-viscosity region, the motion of the solvent is so fast that the conformation of the protein can not follow the solvent motion, and then the time scale of the conformational fluctuation of a protein becomes less sensitive to the solvent viscosity.

Of course, the quite simplified model mentioned above is not enough for the more precise description of the protein dynamics. However, we consider that the HCD model appropriately accounts for the fundamental aspects of our experimental results. The real process may actually be a combination of the HCD and other types of dynamics, such as those controlled by the distribution of the potential barriers. The HCD model was also applied by Murakami and Kushida to analyze the excited-state dynamics of ZnMb in the 170−290 K temperature range observed by the time-resolved fluorescence (TRF) spectroscopy (*43*). They found that the fluorescence spectrum of ZnMb displays a large Stokes shift, which can not be understood by considering only the vibrational relaxation. They attributed this large Stokes shift to a very fast conformational relaxation process from one CS to another occurring within the temporal resolution of 400 ps. Although the amplitude of this relaxation decreases with lowering temperature from 290 K, no slowing down of this process to the time region longer than 400 ps was observed. They explained this phenomenon qualitatively in terms of the HCD model. The conclusion they drew is as follows. The excited-state dynamics of ZnMb consists of two processes. One is a very fast process, which is completed within the temporal resolution of 400 ps and obeys the HCD. The other is a slower process, which is inferred to exist from the fact that the peak position of the fluorescence spectrum of ZnMb depends on the exciting energy. The temporal behavior of the latter process was too slow to be observed in the TRF method. It is probable that the latter process corresponds to the conformational fluctuation process observed in the present TRTHB method. The fast relaxation like the former process does not seem to exist in the ground state of ZnMb, because the experimental results of the TRTHB method have been well-reproduced without introducing such a fast process (*25, 26*). Therefore, the conformational dynamics of ZnMb in the picosecond time region may be different between that in the ground state and that in the excited state, although the dynamics in the nanosecond to microsecond time region is probably similar. This difference possibly results from the nonequilibrium nature of the dynamics observed in the TRF measurement, contrary to the case of the TRTHB measurement in which the essentially equilibrium process is observed.

(C) Comparison of Dynamics between TRTHB and Flash-photolysis. It is quite interesting to compare the conformational dynamics observed by the present TRTHB measurement with that appearing in the data analysis of the flashphotolysis experiment. One must keep in mind, however, that the dynamics observed by the TRTHB is essentially the equilibrium fluctuation while that by the flashphotolysis is the nonequilibrium relaxation. Although it is possible that the fluctuation and the relaxation show the same temporal behavior based on the fluctuation−dissipation theorem, this is the case only when the system is near the equilibrium so that the linear response of the system is valid. Further, at present, we do not know how much the substitution of the central atom of the heme influences the conformational dynamics of Mb. Here, therefore, we will confine ourselves to making a brief comment upon the relation between these differently obtained dynamics.

It has been considered that in the early stage of the CO-rebinding process to Mb, the barrier height dividing the ligated and the unligated state increases with time because of the conformational relaxation of the protein (*22, 23, 44*). This time-dependent barrier mechanism has been accepted to give a plausible explanation for the so-called "inverse temperature effect" in which the geminate-rebinding rate decreases with increasing temperature. Recently, Agmon et al. have succeeded in reproducing the geminate recombination kinetics of MbCO based on their two-dimensional potential model. In this model, the temporal variation of the barrier height is assumed to be induced by the diffusive conformational motion through the protein conformational coordinate, x, whose dynamics is expressed by the Smoluchowski equation with a harmonic potential surface. In their formalism, the relaxation time of this conformational process corresponds to k_BT/Df where D is the diffusivity and f is the constant proportional to the spring constant of the harmonic

potential. Interestingly, this relaxation time estimated by fitting the experimental data for MbCO in W:3G shows a similar temperature dependence with τ_c for ZnMb-W:3G above ~220 K, but is 1−2 orders of magnitude faster than the latter. It was found that the relaxation time estimated in the framework of Agmon et al. lies in the early stage of the fluctuation observed in the present TRTHB study.

Another type of the conformational dynamics has also been introduced, which is considered to concern the ligand escape process from the heme pocket. Tian et al. have estimated the interconversion rate between the so-called open and closed conformers by the double-pulse technique (*12*). The interconversion rate estimated by them also shows a similar temperature dependence with τ_c for ZnMb, but in this case is 1−2 orders of magnitude slower than the latter and lies around the long-time tail of the fluctuation process of ZnMb. Hence, the above-mentioned two types of dynamics derived in the photolysis experiments show temperature dependence similar to that observed in the TRTHB study, although the time scale of both dynamics is somewhat different from the latter. Perhaps these conformational dynamics have a close relationship to that observed for ZnMb. To confirm this relationship, one needs to do further systematic investigation, for example, experiments for ZnMb samples of other species or for site-directed mutant Mb samples.

In the recent work by Huang et al. (*11*), evidence has been given for a relaxation having a temperature and viscosity dependence similar to that observed by the present study. However, it has also been suggested that the relaxation process which induces the temporal broadening of the red edge of the band III persists well below the glass-like transition point of ~200 K. This discrepancy between their results and ours may arise from the fact that they observe the relaxation process, while we do the equilibrium fluctuation.

CONCLUSIONS

The TRTHB studies were carried out for ZnMb solutions with various solvent conditions. The observed temporal changes in both the peak position and width of the THB spectrum were well-explained based on the CC model with an assumption of the harmonic-energy landscape. This shows that the picture of the simple harmonic-energy landscape gives a good description of the real system. A sign of the discrete distribution of the barrier height, that is, the two-phase time evolution of the THB spectra, was also obtained, which may imply hierarchy of the energy landscape. However, such an effect is very small and needs to be confirmed by further detailed observations. As a whole, the nearly single-phase time evolution of the THB spectrum supports the picture of the harmonic potential surface.

From the fitting procedure of the time evolution of the THB spectra, it was found that the time correlation function of the conformational fluctuation of ZnMb is expressed approximately by a stretched-exponential form with a rather small, and almost temperature-independent, β. Further, the correlation time τ_c was found to be linearly dependent on the solvent viscosity regardless of temperature and the solvent condition. The latter phenomenon clearly shows that the glass-like transition of Mb by lowering temperature is induced by the freezing of the solvent. For a qualitative explanation of both the small, temperature-independent β and the linear dependence of τ_c on the solvent viscosity, we employed the HCD model with the postulates that the dynamics in the lowest level in the HCD corresponds in the real system to the motions of the surrounding solvent molecules. On the basis of this interpretation, the following conclusion was drawn.

The rearrangement of the Mb's conformation does not occur until an appropriate configuration of the solvent surrounding Mb is attained in a high-viscosity region. In the low-viscosity region, on the other hand, the conformational dynamics of Mb is constrained less effectively by the solvent degrees of freedom. In a physiological viscosity region, then, τ_c becomes sensitive to the internal friction in the protein rather than to the solvent viscosity. This implies that the dynamical character of the protein will be highly dependent on the type of the protein in such a physiological condition. Hence, we can say that the present TRTHB study has succeeded in revealing a new aspect of the protein dynamics, which is not available from the cryogenic investigations. This underscores the utility of our TRTHB technique for detecting and characterizing the protein dynamics. Recently, we have succeeded in deriving the individuality of the protein dynamics by using this TRTHB method, which is reported in the following paper (*45*).

ACKNOWLEDGMENT

The authors express their gratitude to Prof. Toshiyuki Shikata, to Dr. Osamu Yamamuro of Osaka University, and to Mr. Ming Rong Yao of Rheometric Scientific FE for their help in the measurements of the temperature dependence of the viscosity of the water−diglycerol mixture. They are also grateful to Kuniko Hirata and Ryuzo Ohmukai for helpful advice in preparing the samples.

REFERENCES

1. Frauenfelder, H., Petsko, G. A., and Tsernoglou, D. (1979) *Nature 280*, 558−563.
2. Ansari, A., Berendzen, J., Bowne, S. F., Frauenfelder, H., Iben, I. E. T., Sauke, T. B., Shyamsunder, E., and Young, R. D. (1985) *Proc. Natl. Acad. Sci. U.S.A. 82*, 5000−5004.
3. Iben, I. E. T., Braunstein, D., Doster, W., Frauenfelder, H., Hong, M. K., Johnson, J. B., Luck, S., Ormos, P., Schulte, A., Steinbach, P. J., Xie, A. H., and Young, R. D. (1989) *Phys. Rev. Lett. 62*, 1916−1919.
4. Parak, F., and Frauenfelder, H. (1993) *Physica A 202*, 332−345.
5. Thorn Leeson, D., and Wiersma, D. A. (1995) *Nat. Struct. Biol. 2*, 848−851.
6. Shibata, Y., Kurita, A., and Kushida, T. (1996) *J. Chem. Phys. 104* 4396−4405.
7. Austin, R. H., Beeson, K. W., Eisenstein, L., Frauenfelder, H., and Gunsalus, I. C. (1975) *Biochemistry 14*, 5355−5373.
8. Lambright, D. G., Balasubramanian, S., and Boxer, S. G. (1991) *Chem. Phys. 158*, 249−260.
9. Ansari, A., Jones, C. M., Henry, E. R., Hofrichter, J., and Eaton, W. A. (1992) *Science 256*, 1796−1798.
10. Jackson, T. A., Lim, M., and Anfinrud, P. A. (1994) *Chem. Phys. 180*, 131−140.
11. Huang, J., Ridsdale, A., Wang, J., and Friedman, J. M., (1997) *Biochemistry 36*, 14353−14365.
12. Tian, W. D., Sage, J. T., Champion, P. M., Chien, E., and Sligar, S. G. (1996) *Biochemistry 35*, 3487−3502.
13. Mizutani, Y., and Kitagawa, T. (1997) *Science 278*, 443−446.
14. Ansari, A., Berendzen, J., Braunstein, D., Cowen, B. R., Frauenfelder, H., Hong, M. K., Iben, I. E. T., Johnson, J. B.,

Ormos, P., Sauke, T. B., Scholl, R., Schulte, A., Steinbach, P. J., Vittitow, J., and Young, R. D. (1987) *Biophys. Chem. 26*, 337−355.
15. Ahn, J. S., Kitagawa, T., Kanematsu, Y., Nishikawa, Y., and Kushida, T. (1995) *J. Lumin. 64*, 81−86.
16. Mayer, E. (1994) *Biophys. J. 67*, 862−873.
17. Hagen, S. J., Hofrichter, J., and Eaton, W. A. (1995) *Science 269*, 959−962.
18. Shibata, Y., Kurita, A., and Kushida, T. (1997) *J. Lumin. 72*−*74*, 605−606.
19. Shibata, Y., Kurita, A., and Kushida, T. (1998) *Biophys. J. 75*, 521−527.
20. Kinoshita, S. (1989) *J. Chem. Phys. 91*, 5175−5184.
21. Kidera, A., Inaka, K., Matsushima, M., and Go, N. (1992) *J. Mol. Biol. 225*, 477−486.
22. Agmon, N., and Sastry, G. M. (1996) *Chem. Phys. 212*, 207−219.
23. Sastry, G. M., and Agmon, N. (1997) *Biochemistry 36*, 7097−7108.
24. Kurita, A., Kanematsu, Y., and Kushida, T. (1990) *J. Lumin. 45*, 317−319.
25. Shibata, Y. (1997) Ph.D. Thesis, Osaka University.
26. Shibata, Y., Kurita, A., and Kushida, T. (1996) *J. Lumin. 66*, *67*, 13−18.
27. van der Zwan, G., and Hynes, J. T. (1985) *J. Phys. Chem. 89*, 4181−4188.
28. Kinoshita, S., and Nishi, N. (1988) *J. Chem. Phys. 89*, 6612−6622.
29. Murakami, H., Kinoshita, S., Hirata, Y., Okada, T., and Mataga, N. (1996) *J. Chem. Phys. 97*, 7881−7888.
30. Shibata, Y., and Kushida, T. (1998) *Chem. Phys. Lett. 284*, 115−120.
31. Jäckle, J. (1986) *Rep. Prog. Phys. 49*, 171−231.
32. Steinbach, P. J., Ansari, A., Berendzen, J., Braunstein, D., Chu, K., Cowen, B. R., Ehrenstein, D., Frauenfelder, H., Johnson, J. B., Lamb, D. C., Luck, S., Mourant, J. R., Nienhaus, G. U., Ormos, P., Philipp, R., Xie, A., and Young, R. D. (1991) *Biochemistry 30*, 3988−4001.
33. Hasinoff, B. B. (1977) *Arch. Biochem. Biophys. 183*, 176−188.
34. Morikis, D., Champion, P. M., Springer, B. A., and Sligar, S. G. (1989) *Biochemistry 28*, 4791−4800.
35. Young, R. D., Frauenfelder, H., Johnson, J. B., Lamb, D. C., Nienhaus, G. U., Philipp, R., and Scholl, R. (1991) *Chem. Phys. 158*, 315−327.
36. Kaposi, A. D., Fidy, J., Stavrov, S., and Vanderkooi, J. M. (1993) *J. Phys. Chem. 97*, 6319−6327.
37. Ahn, J. S., Kanematsu, Y., Enomoto, M., and Kushida, T. (1993) *Chem. Phys. Lett. 215*, 336−340.
38. Kurita, A., Matsumoto, K., Shibata, Y., and Kushida, T. (1998) *J. Lumin.*, 295−298.
39. Palmer, R. G., Stein, D. L., Abrahams, E., and Anderson, P. W. (1984) *Phys. Rev. Lett. 53*, 958−961.
40. Kitao, A., Hirata, F., and Go, N. (1991) *Chem. Phys. 158*, 447−472.
41. Kitao, A., Hirata, F., and Go, N. (1993) *J. Phys. Chem. 97*, 10223−10230.
42. Kitao, A., Hirata, F., and Go, N. (1993) *J. Phys. Chem. 97*, 10231−10235.
43. Murakami, H., and Kushida, T. (1996) *Phys. Rev. B. 54*, 978−989.
44. Agmon, N., and Hopfield, J. J. (1983) *J. Chem. Phys. 79*, 2042−2053.
45. Shibata, Y., Takahashi, H., Kaneko, R., Kurita, A., and Kushida, T. (1999) *Biochemistry*, *38*, 1802−1810.

BI9815694